Chemical Engineering Journal 225 (2013) 378–386

Contents lists available at SciVerse ScienceDirect

Chemical Engineering Journal

journal homepage: www.elsevier.com/locate/cej

Evaluation of UV and visible light activity of TiO_2 catalysts for water remediation

Agustina Manassero, María Lucila Satuf, Orlando Mario Alfano *

Instituto de Desarrollo Tecnológico para la Industria Química (Universidad Nacional del Litoral and Consejo Nacional de Investigaciones Científicas y Técnicas), Güemes 3450, 3000 Santa Fe, Argentina

HIGHLIGHTS

- Carbon-doped and undoped TiO_2 catalysts were evaluated under UV and visible light.
- Efficiency parameters involving radiation absorption calculations were computed.
- Optical properties of the catalysts suspensions were measured.
- Carbon-doped sample showed higher efficiency in the visible range.
- Undoped catalyst was more efficient in the UV range.

GRAPHICAL ABSTRACT

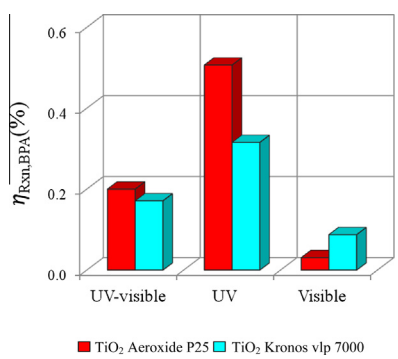

ARTICLE INFO

Article history:
Received 27 December 2012
Received in revised form 23 March 2013
Accepted 26 March 2013
Available online 6 April 2013

Keywords:
Efficiency
TiO_2 optical properties
Photocatalyst
Radiation absorption
Visible activity

ABSTRACT

The photocatalytic activity under UV, visible and UV–visible radiation of two commercial catalysts for water remediation are evaluated and compared in a slurry reactor. Bisphenol A (BPA) was employed as the model pollutant. The activities of the carbon-doped, TiO_2 catalyst Kronos vlp 7000 and, as a reference, the undoped catalyst Aeroxide P25 are compared by means of efficiency parameters: the overall photonic efficiency and the quantum efficiency. For the evaluation of the radiation absorbed by the catalyst suspensions, the optical properties of TiO_2 Kronos vlp 7000 between 300 and 550 nm were measured and reported, as well as the properties of TiO_2 Aeroxide P25 in the range 400–550 nm. Kronos catalyst exhibits absorption in the visible range and was almost three times more efficient than Aeroxide for BPA degradation under this condition. However, under UV radiation, Aeroxide P25 quantum efficiency was about 1.5 times the corresponding value of Kronos. Similar BPA photonic and quantum efficiencies were obtained under UV–visible radiation with both commercial catalysts.

1. Introduction

Heterogeneous photocatalysis has been extensively applied to remove refractory pollutants from the aquatic environment. TiO_2 is one of the most widely used photocatalysts because it is stable, inexpensive and nontoxic. However, to be excited and capable of photo-oxidation, TiO_2 must be irradiated with UV light. Because UV radiation only accounts for 4% of the solar spectrum, the photocatalytic efficiency of pure TiO_2 under sunlight is very low. To extend the use of TiO_2 to the visible light region (which represents 45% of the solar spectrum) and take advantage of solar energy, different strategies have been developed [1]. One alternative is the doping of the catalyst with carbon, which produces new energy states in the TiO_2 band gap and allows photo-activation with visible light [2–6]. Recently, the degradation of a cyanotoxin under UV and visible light has been investigated using undoped, nitrogen-doped and carbon-doped TiO_2 catalysts [7]. Nevertheless, comparison of photocatalysts employing efficiency parameters has not been reported until now. The calculation of

* Corresponding author. Tel.: +54 342 4511546; fax: +54 342 4511170.
E-mail address: alfano@santafe-conicet.gov.ar (O.M. Alfano).

1385-8947/$ - see front matter © 2013 Elsevier B.V. All rights reserved.
http://dx.doi.org/10.1016/j.cej.2013.03.097

Nomenclature

A_w	reactor window area (cm^2)
BPA	bisphenol A
C	molar concentration (mol cm^{-3})
C_m	catalyst mass concentration (g cm^{-3})
e^a	local volumetric rate of photon absorption (Einstein cm^{-3} s^{-1})
EDC	endocrine disrupting chemical
g	asymmetry factor (dimensionless)
I	radiation intensity (Einstein cm^{-2} sr^{-1} s^{-1})
L_R	reactor length (cm)
p	scattering phase function
q_w	incident radiation flux (Einstein s^{-1} cm^{-2})
RTE	radiative transfer equation
r	reaction rate (mol cm^{-3} s^{-1})
t	time (s)
V	volume (cm^3)
x	axial coordinate (cm)
$\boldsymbol{x}$	position vector (cm)

Greek letters

β	volumetric extinction coefficient (cm^{-1})
β^*	specific coefficient of extinction (cm^2 g^{-1})
ε	hold-up (dimensionless)
η	overall photonic efficiency (mol $Einstein^{-1}$)
η_{Rxn}	quantum efficiency of reaction (mol $Einstein^{-1}$)
η_{Abs}	photon absorption efficiency (dimensionless)
κ	volumetric absorption coefficient (cm^{-1})
κ^*	specific coefficient of absorption (cm^2 g^{-1})
μ	direction cosine of the ray for which the RTE is written
μ'	direction cosine of an arbitrary ray before scattering
μ_0	cosine of the angle between the direction of the incident and the scattered rays
μ_c	cosine of the critical angle
σ	volumetric scattering coefficient (cm^{-1})
σ^*	specific coefficient of scattering (cm^2 g^{-1})
Γ_w	global reflection coefficient of the reactor windows
θ	spherical coordinate (rad)
θ_c	critical angle (rad)
τ	optical thickness of the reactor (dimensionless)
ω	albedo (dimensionless)
Ω	unit vector in the direction of radiation propagation

Subscripts

BPA	bisphenol A
λ	dependence on wavelength
HG	Henyey and Greenstein
L	liquid phase
R	reactor
T	total
Tk	tank
0	initial condition; also, relative to the reactor window at $x = 0$

Special symbols

$\langle\rangle$	denotes average value over a given space

efficiency parameters involves the measurement and computation of the radiation reaching the catalyst particles and the radiation effectively absorbed by them [8–13].

In this paper, Bisphenol A (BPA), a known endocrine disrupting chemical (EDC), is employed as the model compound in degradation experiments. BPA is used in the fabrication of polycarbonate plastics, food cans, plastic packaging, dental sealants and water pipes [14]. It is released into the aquatic environment from industrial discharges, landfill leachate and water streams containing plastic debris [15]. Several studies have reported that exposure to BPA is potentially harmful to human health [16]. Because many EDCs, including BPA, can only be partially removed by conventional water treatment systems, there is a need to evaluate alternative treatment processes to prevent the release of EDCs into natural waters [17]. Previous studies have demonstrated the effectiveness of heterogeneous photocatalysis for removing BPA in aqueous media employing UV radiation [18–22]. Furthermore, different approaches to remove BPA under visible radiation have also been reported. In this sense, TiO_2 doped with non-metals was used to extend the absorption of TiO_2 to the visible light region [23,24].

The aim of this paper is to objectively compare the degradation of BPA under UV, visible and UV–visible radiation using undoped and carbon-doped TiO_2 in a slurry reactor. Two commercial catalysts were assayed: Aeroxide P25 and carbon-doped Kronos vlp 7000. The performances of both catalysts were evaluated by two parameters: the overall photonic efficiency (η), which relates the moles of BPA degraded per mol of incident photons, and the quantum efficiency of reaction (η_{Rxn}), i.e. moles of BPA degraded per mol of photons absorbed. To calculate the photon absorption in the reactor, the optical properties of the catalysts are needed. The optical properties of Aeroxide P25 in the UV range have already been measured [25,26]. However, the optical properties of Kronos vlp 7000 in the UV–visible range have not yet been published, and are presented in this work. Additionally, the properties of Aeroxide P25 in the visible range are also measured and reported. Photon absorption was calculated by solving the radiative transfer equation (RTE).

2. Materials and methods

2.1. Materials

Bisphenol A (BPA) was obtained from Aldrich ($\geqslant$99%, molecular formula $C_{15}H_{16}O_2$). The commercial photocatalysts used in this study were: TiO_2 Aeroxide P25 (Evonik Degussa GmbH, Germany) and TiO_2 Kronos vlp 7000 (Kronos Titan GmbH, Germany). The physical properties of the catalysts are summarized in Table 1. Deionized and doubled-distilled water was used to prepare all solutions.

2.2. Experimental set up and procedure

A total of six experiments, by duplicate, were conducted to evaluate the efficiency of both photocatalysts under three irradiation conditions: UV, visible and UV–visible.

Table 1
Physical properties of the catalysts.

Photocatalyst	Mean particle size (nm)	Specific surface area (BET) (m^2 g^{-1})	Crystal structure
TiO_2 Aeroxide P25	21	50 ± 15	Anatase (80%) and rutile (20%)
TiO_2 Kronos vlp 7000	15	>250	Anatase

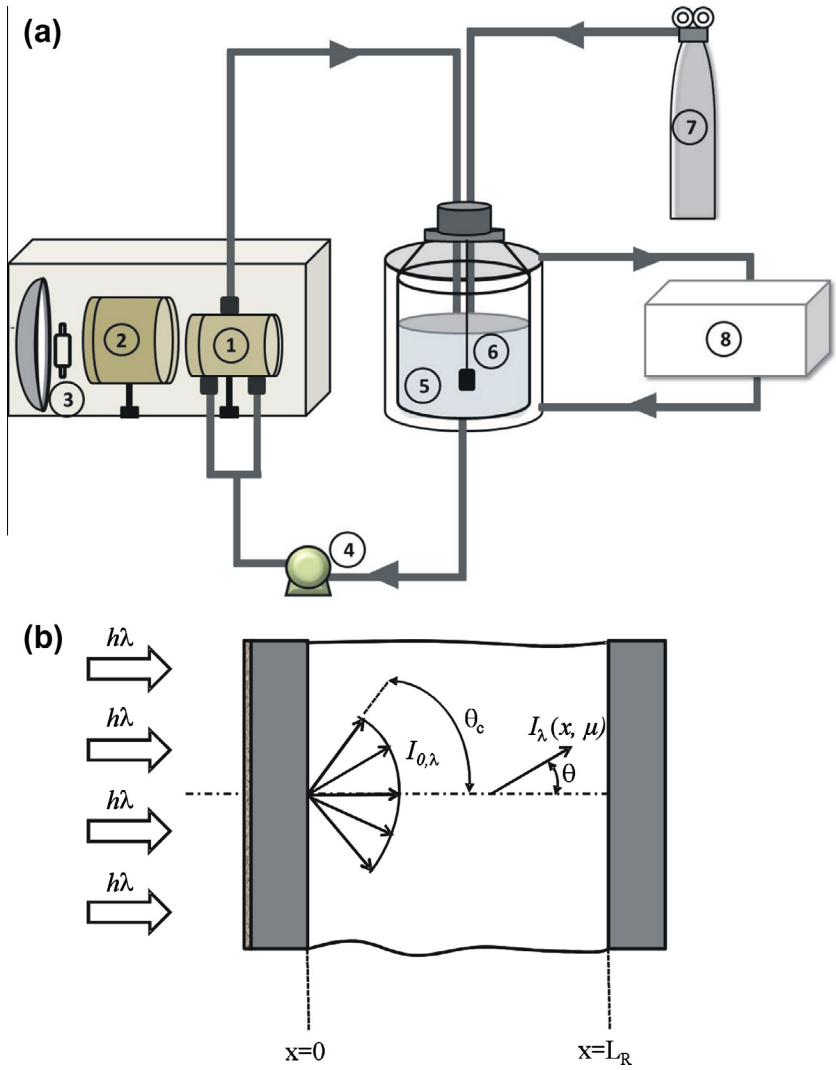

Fig. 1. (a) Schematic representation of the experimental setup: 1-reactor, 2-filter, 3-lamp, 4-pump, 5-tank, 6-thermometer, 7-oxygen and 8-thermostatic bath. (b) Coordinate system for the one-dimensional, one-directional radiation model.

The experimental set up is schematically represented in Fig. 1a. Experiments were carried out in a cylindrical glass reactor with two circular flat windows. The illuminated window was made of borosilicate ground glass. Radiation was provided by a halogenated mercury lamp Powerstar HQI from OSRAM, with emission in the UV and visible range (350–550 nm), placed at the focal axis of a parabolic reflector. The distance between the lamp and the reactor was 24 cm. The reactor was operated in a closed recirculating circuit driven by a peristaltic pump (Masterflex®, flow rate 1.5 L min^{-1}). The system was completed with a storage tank equipped with a water-circulating jacket to ensure isothermal conditions during the reaction time (20 °C). The tank contained a device for withdrawal of samples, a thermometer, and a gas inlet for oxygen supply. A filter containing a solution of $CoSO_4$ or $NaNO_2$ was interposed between the reactor and the lamp to alternatively avoid visible or UV radiation, respectively. The length of the filter container was 12 cm. Fig. 2 shows the spectral distribution of radiation at the reactor window with the different filters. UV radiation that reached the reactor when the filter compartment was filled with $CoSO_4$ was comprised between 350 and 420 nm, and represented ca. 25% of the total emission of the lamp. When the $NaNO_2$ filter was employed, visible radiation that reached the reactor was comprised between 410 and 550 nm, representing almost 75% of the total energy emitted. To carry out experiments employing the whole lamp spectrum (UV and visible range), the filter holder was filled with distilled water. Table 2 summarizes the dimensions of the reactor and the characteristics of the lamp.

For each experiment, the suspension was prepared by dissolving a defined mass of BPA and photocatalyst (Aeroxide P25 or Kronos vlp 7000) in a total volume of 500 cm^3. The initial BPA concentration was always 20 mg L^{-1} and the catalyst concentration was 0.5 g L^{-1}. The solution pH was adjusted to 7.0 by adding the appropriate volume of NaOH 0.1 N [27]. The suspension was sonicated for 30 min and then it was added to the tank. The reacting mixture was circulated in the reactor for 120 min to achieve the adsorption equilibrium between BPA and the catalyst. During this time, the suspension was saturated with pure oxygen by intense bubbling and the lamp was turned on to achieve stabilization of the radiation emission. To prevent the arrival of radiation at the reactor, a shutter was placed between the lamp and the reactor window. When the system was stabilized and adsorption equilibrium was reached, the first sample was taken ($t = 0$) and then the shutter was removed. Throughout the reaction, the system was maintained under overpressure of oxygen to guarantee the renewal of the oxygen consumed. A control experiment to verify the absence of BPA evaporation in the system was carried out. The suspension was recirculated and bubbled with oxygen during 6 h. No detectable changes in the concentration of BPA were observed. Each

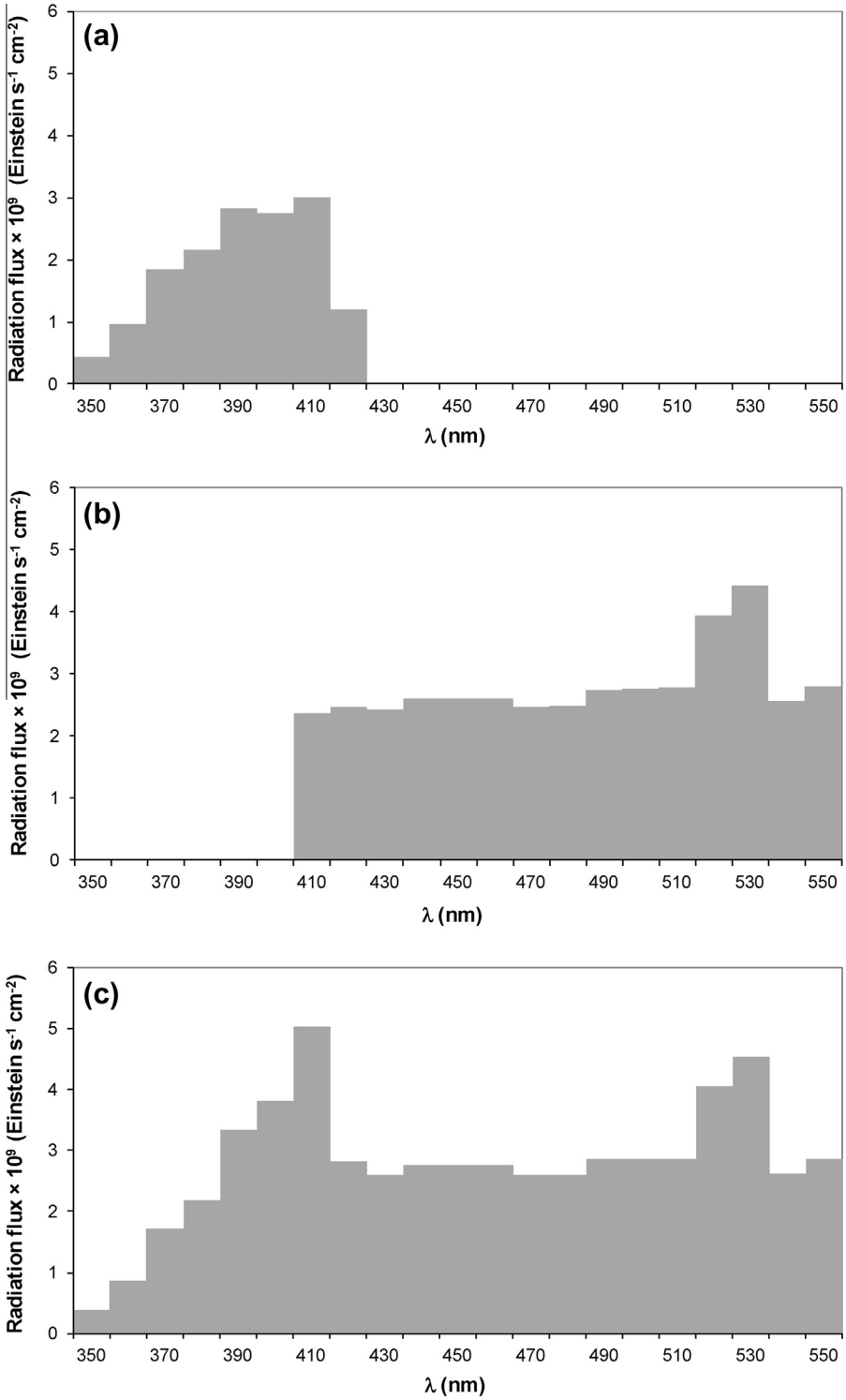

Fig. 2. Spectral distribution of radiation with different filters: (a) $CoSO_4$ filter; (b) $NaNO_2$ filter; and (c) water filter.

experiment lasted 450 min and sampling was done every 90 min. TiO_2 suspension samples were separated out by centrifugation and filtered through a 0.02 μm (Anotop 25) to remove the catalyst particles before analysis. A set of control experiments was carried out to evaluate direct photolysis under the three irradiation conditions employed in the study. No significant changes were detected in the concentration of BPA after 450 min of irradiation.

2.3. Analysis

The BPA concentration was measured by HPLC with a UV detector using a Waters chromatograph provided with a RP C-18 column (XTerra®). The mobile phase was a binary mixture of acetonitrile–water (50:50) at a flow rate of 1 mL min^{-1}. Absorbance detection was made at 278 nm [27].

Table 2
Dimensions and main characteristics of the reactor and lamp.

Component	Parameter	Value
Reactor	Inner diameter (cm)	5.0
	Length (cm)	2.75
	Volume (cm^3)	54
	Suspension volume (cm^3)	500
Lamp	Nominal power (W)	150
	Height (mm)	132
	Diameter (mm)	23
	UV radiation flux (Einstein s^{-1} cm^{-2}) (350–420 nm)	1.52×10^{-8}
	Visible radiation flux (Einstein s^{-1} cm^{-2}) (410–550 nm)	4.20×10^{-8}
	UV–visible radiation flux (Einstein s^{-1} cm^{-2}) (350–550 nm)	5.88×10^{-8}

3. Calculation of efficiency parameters

In photocatalytic reactions, the overall photonic efficiency η relates the number of molecules of pollutant degraded with the number of incident photons during a defined period of time, over a defined spectral range. In real situations, not all the incident radiation is absorbed by the catalyst. Photons might be scattered out of the reactor and lost. This type of loss can be quantified by the photon absorption efficiency η_{Abs} which relates the number of photons effectively absorbed by the catalyst with the total number of incident photons [10]:

$$\eta_{Abs} = \frac{\langle e^a(x)\rangle_{V_R} V_R}{\langle q_w(x)\rangle_{A_w} A_w} \tag{1}$$

where $\langle e^a(x)\rangle_{V_R}$ is the local volumetric rate of photon absorption (LVRPA) averaged over the reactor volume, V_R, and $\langle q_w(x)\rangle_{A_w}$ represents the incident radiation flux averaged over the reactor window area, A_w.

In turn, the quantum efficiency of reaction (η_{Rxn}) is the ratio between the number of molecules of pollutant degraded to the number of photons absorbed by the photocatalyst, during a defined period of time and over a defined range of wavelengths. The quantum efficiency of BPA can be expressed as [10]:

$$\eta_{Rxn,BPA} = \frac{\langle r_{BPA}(x,t_0)\rangle_{V_R}}{\langle e^a(x)\rangle_{V_R}} \tag{2}$$

where $\langle r_{BPA}(x,t_0)\rangle_{V_R}$ is the initial volumetric rate of BPA degradation averaged over the reactor volume.

Particularly, the overall photonic efficiency for the BPA photocatalytic degradation η_{BPA} can be expressed as follows [13]:

$$\eta_{BPA} = \eta_{Abs}\eta_{Rxn,BPA} = \frac{\langle r_{BPA}(x,t_0)\rangle_{V_R} V_R}{\langle q_w(x)\rangle_{A_w} A_w} \tag{3}$$

In the present study, $\langle r_{BPA}(x,t_0)\rangle_{V_R}$ was obtained from experimental information. For this purpose, we considered the BPA mass balance in the system, making the following assumptions [10]:

(i) there is a differential conversion per pass in the reactor,
(ii) the system is perfectly mixed,
(iii) there are no mass transport limitations, and
(iv) the chemical reaction occurs only at the solid–liquid interface,

Therefore, the mass balance for BPA is:

$$\varepsilon_L \left.\frac{dC_{BPA}(t)}{dt}\right|_{Tk} = -\frac{V_R}{V_T}\langle r_{BPA}(x,t)\rangle_{V_R} \tag{4}$$

where ε_L is the liquid hold-up ($\varepsilon_L \approx 1$), C_{BPA} is the molar concentration of BPA, t denotes the reaction time and Tk refers to the tank. From the mass balance, it can be derived the expression for calculating the initial reaction rate:

$$\langle r_{BPA}(x,t_0)\rangle_{V_R} = -\varepsilon_L \frac{V_T}{V_R}\lim_{t\to t_0}\left(\frac{C_{BPA}(t) - C_{BPA}(t_0)}{t - t_0}\right)_{Tk} \tag{5}$$

For every experimental run, $\left(\frac{C_{BPA}(t)-C_{BPA}(t_0)}{t-t_0}\right)_{Tk}$ was obtained from the initial slope of the plot of C_{BPA} versus time.

Besides, $\langle q_w(x)\rangle_{A_w}$ was experimentally measured by potassium ferrioxalate actinometry [28].

The LVRPA was calculated by solving the RTE in the heterogeneous reactor. To solve the RTE, it is necessary to know the optical properties of the photocatalysts suspensions: the spectral absorption coefficient (κ_λ), the spectral scattering coefficient (σ_λ) and the scattering phase function (p_λ) [29,25]. The Henyey and Greenstein phase function ($p_{HG,\lambda}$) was adopted [30]:

$$p_{HG,\lambda}(\mu_0) = \frac{1 - g_\lambda^2}{(1 + g_\lambda^2 - 2g_\lambda\mu_0)^{3/2}} \tag{6}$$

where g_λ is a free parameter called the asymmetry factor, and μ_0 represents the cosine of the angle between the direction of the incident and the scattered rays.

4. Optical properties of the photocatalysts

The optical properties of TiO_2 Aeroxide P25 from 300 to 400 nm were previously reported [26]. The properties of Aeroxide P25 in the visible range, from 400 to 550 nm, and those corresponding to Kronos vlp 7000 from 300 to 550 nm, were determined for the first time in this study. The procedure involved experimental measurements and theoretical modeling.

Experimental measurements of absorbance, diffuse reflectance and diffuse transmittance of the TiO_2 suspensions were made by an Optronic OL series 750 spectroradiometer equipped with an OL 740-70 integrating sphere reflectance attachment. Rectangular quartz cells with an optical path (L) of 1 mm were employed. Suspensions of different catalyst concentrations were prepared in distilled water, ranging from 0.1 to 0.5 g L^{-1}. The catalysts were previously oven-dried at 120 °C for 3 h. Readings were recorded every 10 nm.

4.1. Calculation of the extinction coefficient

For each wavelength and each catalyst concentration, the extinction coefficient β_λ ($\beta_\lambda = \sigma_\lambda + \kappa_\lambda$) was calculated from absorbance readings (ABS_λ) of the TiO_2 suspensions as $\beta_\lambda = 2.303\ ABS_\lambda/L$. Measurements were carried out under specially designed

Table 3
BPA degradation rates for TiO_2 Aeroxide P25 and Kronos vlp 7000 under different irradiation conditions.

Irradiation range	Aeroxide P25		Kronos vlp 7000	
	$\langle r_{BPA}(x,t_0)\rangle_{V_R} \times 10^{11}$ (mol cm^{-3} s^{-1})	R^2	$\langle r_{BPA}(x,t_0)\rangle_{V_R} \times 10^{11}$ (mol cm^{-3} s^{-1})	R^2
UV	1.87 ± 0.19	0.9964	1.46 ± 0.14	0.9706
Visible	0.32 ± 0.08	0.9918	1.13 ± 0.12	0.9989
UV–visible	2.90 ± 0.36	0.9973	3.10 ± 0.43	0.9468

conditions to minimize the collection of the scattered rays by the detector [25]. Then, the extinction coefficients per unit catalyst mass concentration C_m (i.e., specific extinction coefficients, β^*_λ) were obtained from the slope of a standard linear regression of the plots of β_λ versus C_m.

4.2. Calculation of the absorption and scattering coefficients and the asymmetry factor

Diffuse reflectance and diffuse transmittance measurements of the TiO_2 suspensions were made following the procedure described in [26]. Experimental information was then compared with modeling results. Simulation values were calculated by solving the RTE in the spectrophotometric sample cell, with two unknown parameters: the spectral albedo $\omega_\lambda = \sigma_\lambda/\beta_\lambda$ and g_λ. A nonlinear, multiparameter regression procedure (a modified Levenberg–Marquardt method) was employed to adjust theoretical values to experimental information. The optimization program rendered the values of ω_λ and g_λ that minimize the differences between model predictions and experimental data. Therefore, knowing that $\omega_\lambda = \sigma_\lambda/\beta_\lambda$ and using the values of β_λ obtained experimentally, σ_λ was determined for each wavelength and catalyst concentration. Finally, through the relationship $\beta_\lambda = \sigma_\lambda + \kappa_\lambda$, κ_λ was obtained. The specific coefficients of absorption (κ^*_λ) and scattering (σ^*_λ) were calculated from the slopes of the standard linear regressions of the plots of κ_λ and σ_λ versus C_m.

5. Radiation model in the reactor

To calculate the local volumetric rate of photon absorption inside the photoreactor, the RTE was solved. For this purpose, the following assumptions were made (Fig. 1b) [31]:

(i) The catalyst particles produce the extinction of radiation mainly along the axial coordinate x; thus, the propagation of the radiation can be modeled with a single spatial variable.
(ii) The ground glass window ensures diffuse incoming radiation at the reactor. Therefore, radiation can be modeled with one angular variable (θ).

These assumptions allow the application of the one-dimensional, one-directional radiation transport model to solve the RTE inside the photocatalytic reactor:

$$\frac{\mu}{\beta_\lambda}\frac{\partial I_\lambda(x,\mu)}{\partial x} + I_\lambda(x,\mu) = \frac{\omega_\lambda}{2}\int_{\mu'=-1}^{1} I_\lambda(x,\mu')p_\lambda(\mu,\mu')d\mu' \quad (7)$$

where I_λ is the spectral radiation intensity; λ represents the radiation wavelength; μ, the direction cosine of the ray for which the RTE is written ($\mu = \cos\theta$); and μ', the cosine of an arbitrary ray before scattering.

The boundary conditions at the irradiated window ($x = 0$) and at the rear window ($x = L_R$) are:

$$I_\lambda(0,\mu) = \Gamma_{w,\lambda}(-\mu)I_\lambda(0,-\mu) \quad 0 \leqslant \mu < \mu_c \quad (8)$$

$$I_\lambda(0,\mu) = I_{0,\lambda} + \Gamma_{w,\lambda}(-\mu)I_\lambda(0,-\mu) \quad \mu_c \leqslant \mu < 1 \quad (9)$$

$$I_\lambda(L_R,-\mu) = \Gamma_{w,\lambda}(\mu)I_\lambda(L_R,\mu) \quad 0 \leqslant \mu \leqslant 1 \quad (10)$$

where $\Gamma_{w,\lambda}$ represents the global wall reflection coefficient, μ_c is the cosine of the critical angle θ_c, and I_0 corresponds to the intensity of radiation coming from the lamp. $\Gamma_{w,\lambda}$, was calculated as reported in [32].

To obtain the spectral radiation intensity at each point and each direction inside the photoreactor, the RTE was solved applying the Discrete Ordinate Method (DOM). 3000 spatial points and 50 directions were used in the numerical solution. The DOM transforms the integro-differential expression of the RTE into a system of finite differences algebraic equations that can be solved by numerical computation. Once the intensities were obtained, the LVRPA was calculated according to:

$$\text{LVRPA} = e^a(x) = \int_\lambda \kappa_\lambda \int_{\Omega=4\pi} I_{\lambda,\Omega}(x)d\Omega d\lambda \quad (11)$$

Finally, for the one-dimensional model, the local volumetric rate of photon absorption averaged over the reactor volume was computed as:

$$\langle e^a(x)\rangle_{V_R} = \frac{1}{V_R}\int_{V_R} e^a(x)dV \quad (12)$$

6. Results and discussion

6.1. Optical properties of the TiO_2 suspensions

Fig. 3 presents the specific absorption and scattering coefficients for Aeroxide P25 and Kronos vlp 7000 as a function of wavelength. For $\lambda < 380$ nm (UV region), κ^*_λ of Aeroxide P25 is greater than that of Kronos, and this difference increases at shorter wavelengths. In the visible region, the absorption of Aeroxide falls to almost 0, while the absorption coefficient of Kronos decreases to acquire a practically constant value (which is almost three times greater than that of Aeroxide). It is important to remark that κ^*_λ of Kronos never becomes zero in the wavelength range evaluated. This behavior is attributed to the carbon doped modification that makes TiO_2 Kronos vlp 7000 capable of absorbing photons in the visible range [2].

At wavelengths longer than 320 nm for Aeroxide P25 and 350 nm for Kronos, the scattering coefficients are greater than the absorption coefficients. In addition, σ^*_λ of Aeroxide is always greater than that of Kronos, being this difference more noticeable at shorter wavelengths. Moreover, the spectral behavior of the scattering coefficient is different for both catalysts: For Aeroxide P25, this coefficient presents a maximum at 370 nm and then slowly decreases at longer wavelengths. For Kronos vlp 7000, σ^*_λ increases in the wavelength range between 320 and 370 nm and then takes a practically constant value.

Finally, for the asymmetry factor g_λ, both catalysts present positive values, comprised between ≈0.42 and ≈0.86, indicating a preferential forward direction of the scattered radiation. The values of g_λ, along with the values of β^*_λ, κ^*_λ and σ^*_λ, are presented in Tables S1 and S2 (Supporting information).

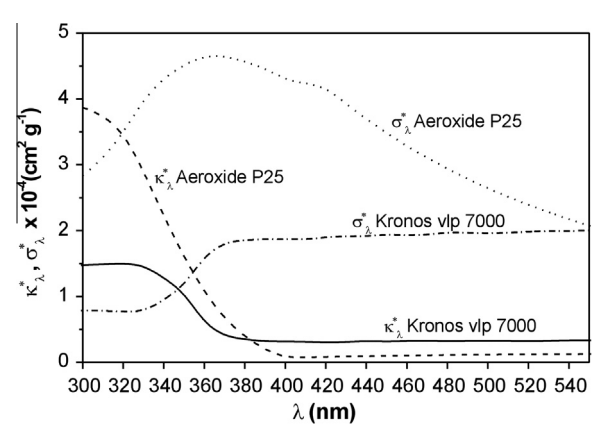

Fig. 3. Spectral distribution of the specific absorption and scattering coefficients for Aeroxide P25 and Kronos vlp 7000.

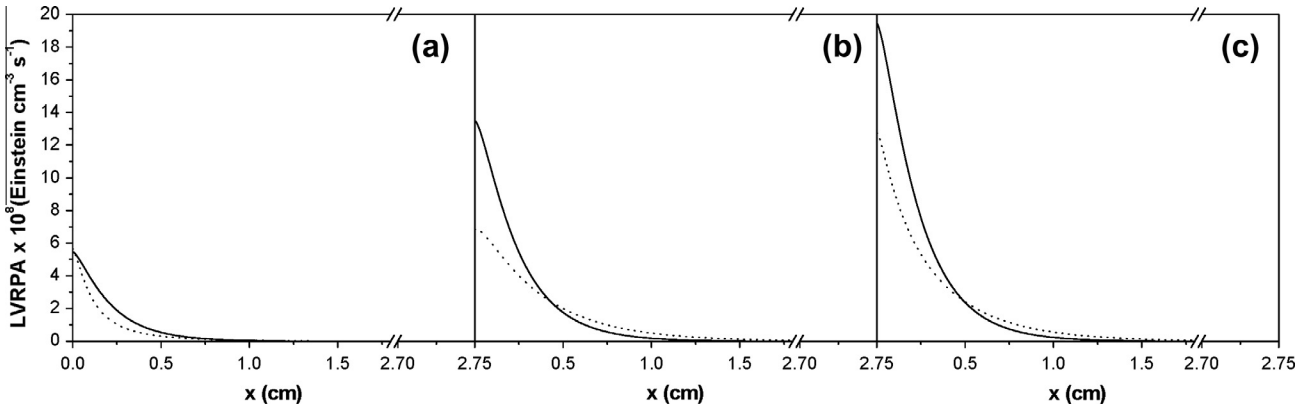

Fig. 4. LVRPA profiles for TiO_2 Aeroxide P25 (short dash lines) and TiO_2 Kronos vlp 7000 (solid lines) under different irradiation ranges: (a) UV radiation; (b) visible radiation; and (c) UV–visible radiation.

Table 4
Photon absorption rate and efficiencies for TiO_2 Aeroxide P25 under different irradiation conditions.

Irradiation range	$\langle e^a(x)\rangle_{V_R} \times 10^8$ (Einstein cm^{-3} s^{-1})	η_{Abs} (%)	$\eta_{Rxn,BPA}$ (%)	η_{BPA} (%)
UV	0.37	67.0	0.51	0.34
Visible	1.04	68.2	0.031	0.021
UV–visible	1.45	67.9	0.20	0.14

Table 5
Photon absorption rate and efficiencies for TiO_2 Kronos vlp 7000 under different irradiation conditions.

Irradiation range	$\langle e^a(x)\rangle_{V_R} \times 10^8$ (Einstein cm^{-3} s^{-1})	η_{Abs} (%)	$\eta_{Rxn,BPA}$ (%)	η_{BPA} (%)
UV	0.46	83.3	0.32	0.26
Visible	1.29	84.7	0.088	0.074
UV–visible	1.81	84.7	0.17	0.15

6.2. Radiation distribution inside the reactor

The LVRPA profiles for both catalysts studied, at a concentration of 0.5 g L^{-1}, under UV, visible and UV–visible radiation, are shown in Fig. 4. For the three irradiation ranges and for both catalysts, the optical thickness τ of the reactor ($\tau = \beta L_R$) was sufficient to avoid the lost of radiation through the rear window, i.e. no radiation was transmitted through the reactor. In all cases, more than 90% of the total absorbed radiation was achieved in the space comprised between the irradiated window and $x = 1$ cm. In the UV region, both catalysts presented similar absorption profiles. On the contrary, when the reactor was illuminated with visible and UV–visible radiation, Kronos catalyst presented higher absorption near the irradiated window, and a steeper decrease inside the reactor. Aeroxide TiO_2 absorption profiles were smoother, with more penetration in the reactor space.

The photon absorption efficiency η_{Abs} is mainly determined by the albedo ω and the optical thickness τ. In the limit of an only-scattering medium, $\omega = 1$ and the fraction of photons absorbed is null ($\eta_{Abs} = 0$). For an only-absorbing medium, $\omega = 0$ and, for a value of τ sufficiently high, the efficiency of absorption is maximum and all the incident radiation is absorbed ($\eta_{Abs} = 1$). In this study, the wavelength average value of $\bar{\omega}$ for each catalyst did not vary significantly with the irradiation range. Therefore, as reported in Tables 4 and 5, the calculated efficiency of photon absorption was around 68% for Aeroxide P25 and 84% for Kronos, for the three irradiation ranges. In all cases, the radiation lost was due to the scattering out through the front window.

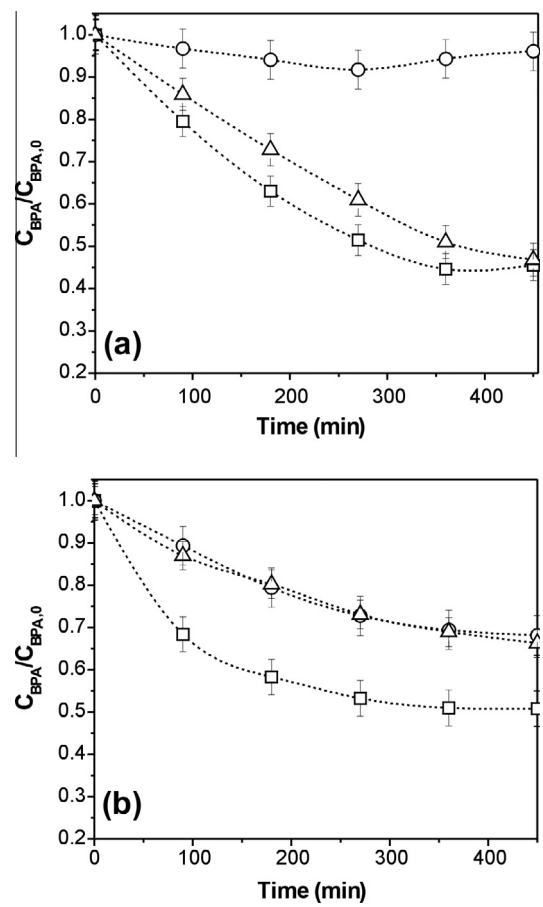

Fig. 5. Time evolution of BPA concentration under different irradiation conditions: △: UV radiation, ○: visible radiation, and □: UV–visible radiation. (a) TiO_2 Aeroxide P25. (b) TiO_2 Kronos vlp 7000.

6.3. BPA degradation

BPA degradation curves with TiO_2 Aeroxide P25 and Kronos vlp 7000 are shown in Fig. 5. Experiments were carried out at a catalyst

concentration of 0.5 g L^{-1}. The plots C_{BPA} versus time were fitted with exponential equations (fittings are not shown in the figure) and initial reaction rates were determined by calculating the slopes of the fitting curves at time equals 0. The values of the reaction rates, with the corresponding 95% confidence interval and R^2 are presented in Table 3.

For Aeroxide P25, degradation under visible light was very low [6]. Considerably higher reaction rates were obtained with UV and UV–visible radiation.

The results obtained with Kronos vlp 7000 demonstrated that carbon-doped TiO_2 is effectively activated by visible radiation. Degradation of BPA under visible light was significant, yielding similar reaction rates under UV and visible radiation. The initial reaction rate of Kronos was over three times that of Aeroxide under visible light.

6.4. Quantum efficiency and overall photonic efficiency

Tables 4 and 5 report the local volumetric rate of photon absorption averaged over the reactor volume, and the corresponding values of η_{Abs}, $\eta_{Rxn,BPA}$ and η_{BPA} for each irradiation condition (UV, visible and UV–visible) and for each catalyst assayed. The overall photonic efficiency represents a sort of lower limit of the quantum efficiency, given that the denominator of η_{BPA} (incident radiation) is always higher than that of $\eta_{Rxn,BPA}$ (absorbed radiation) [33]. In our particular case, because each catalyst absorbed similar percentages of radiation under the three wavelengths ranges, η_{BPA} and $\eta_{Rxn,BPA}$ presented equivalent variations, i. e. for Aeroxide, photonic efficiency values were 68% of the quantum efficiency. And for Kronos, η_{BPA} represented 84% of $\eta_{Rxn,BPA}$. Therefore, only results of quantum efficiencies are discussed here.

Although efficiency values are below 1%, they are in the range of the expected values for the photocatalytic degradation of organic compounds in water [1]. Under UV radiation, Aeroxide quantum efficiency was about 1.5 times the corresponding value of Kronos. The lowest efficiencies were obtained with visible radiation; however Kronos proved to be more efficient for BPA degradation under this irradiation range, achieving a $\eta_{Rxn,BPA}$ ca. three times greater than Aeroxide. Although Aeroxide P25 absorbed almost 68% of the incident visible radiation, only a low percentage of this energy was employed in the photocatalytic process, giving a very low efficiency value (0.031%). The slight visible absorption of Aeroxide P25 could be attributed to impurities in the catalyst because it is well known that the absorption limits of pure TiO_2 anatase and rutile are 380 nm and 400 nm, respectively. Under UV–visible radiation, both catalysts rendered similar efficiencies.

It should be stressed, that previous research [34] clearly showed that photocatalytic activity is substrate-dependant. Therefore, the performance of a photocatalyst to degrade a particular compound cannot be extrapolated to substrates of different chemical structure and/or properties. Besides, equally important is the correct assessment of the energy absorbed in the reactor, taking into account the spectral distribution of the incident radiation and the optical properties of the catalyst. If this information is not provided, efficiency results obtained with different devices (reactors, lamps, filters) cannot be compared.

7. Conclusions

Degradation of BPA using two commercial TiO_2 photocatalysts under UV, visible and UV–visible radiation was investigated. zEfficiency parameters were computed to objectively compare the performances of the catalysts. To evaluate the volumetric rate of photon absorption averaged over the reactor volume, the optical properties of TiO_2 Kronos and Aeroxide P25 were measured. The Kronos sample exhibits absorption in the visible region, and a considerable photocatalytic activity was observed under this irradiation range. Nevertheless, the efficiency obtained was very low compared to that achieved in the UV range. On the other hand, under UV radiation, the BPA quantum efficiency with Aeroxide P25 was about 1.5 times that obtained with Kronos vlp 7000. Finally, under UV–visible radiation, comparable photonic and quantum efficiencies were obtained with both commercial photocatalysts.

Although considerable advances have been made, future research efforts should be devoted to develop more efficient photocatalysts under visible light, thus making photocatalysis a sustainable process employing solar energy.

Acknowledgements

The authors are grateful to Universidad Nacional del Litoral (UNL), Consejo Nacional de Investigaciones Científicas y Técnicas (CONICET), and Agencia Nacional de Promoción Científica y Tecnológica (ANPCyT) for financial support. We also thank Antonio C. Negro for his valuable help during the experimental work.

Appendix A. Supplementary material

Supplementary data associated with this article can be found, in the online version, at http://dx.doi.org/10.1016/j.cej.2013.03.097.

References

[1] M. Pelaez, N.T. Nolan, S.C. Pillai, M.K. Seery, P. Falaras, A.G. Kontos, P.S.M. Dunlop, J.W.J. Hamilton, J.A. Byrne, K. ÓShea, M.H. Entezari, D.D. Dionysiou, A review on the visible light active titanium dioxide photocatalysts for environmental applications, Appl. Catal. B 125 (2012) 331–349.
[2] S. Sakthivel, H. Kisch, Daylight photocatalysis by carbon-modified titanium dioxide, Angew. Chem. Int. Ed. 42 (2003) 4908–4911.
[3] H. Irie, S. Washizuka, K. Hashimoto, Hydrophilicity on carbon-doped TiO_2 thin films under visible light, Thin Solid Films 510 (2004) 21–25.
[4] K. Nagaveni, M.S. Hegde, N. Ravishankar, G.N. Subbanna, G. Madras, Synthesis and structure of nanocrystalline TiO_2 with lower band gap showing high photocatalytic activity, Langmuir 20 (2004) 2900–2907.
[5] D.B. Hamal, K.J. Klabunde, Synthesis, characterization, and visible light activity of new nanoparticle photocatalysts based on silver, carbon, and sulfur-doped TiO_2, J. Colloid Interface Sci. 311 (2007) 514–522.
[6] S. Goldstein, D. Behar, J. Rabani, Mechanism of visible light photocatalytic oxidation of methanol in aerated aqueous suspensions of carbon-doped TiO_2, J. Phys. Chem. C 112 (2008) 15134–15139.
[7] T.M. Triantis, T. Fotiou, T. Kaloudis, A.G. Kontos, P. Falaras, D.D. Dioniysiou, M. Pelaez, A. Hiskia, Photocatalytic degradation and mineralization of microcystin-LR under UV-A, solar and visible light using nanostructured nitrogen doped TiO_2, J. Hazard. Mater. 211–212 (2012) 196–202.
[8] N. Serpone, Relative photonic efficiencies and quantum yields in heterogeneous photocatalysis, J. Photochem. Photobiol. A: Chem. 104 (1997) 1–12.
[9] M. Salaices, B. Serrano, H.I. de Lasa, Experimental evaluation of photon absorption in an aqueous TiO_2 slurry reactor, Chem. Eng. J. 90 (2002) 219–229.
[10] M.L. Satuf, R.J. Brandi, A.E. Cassano, O.M. Alfano, Quantum efficiencies of 4-chlorophenol photocatalytic degradation and mineralization in a well-mixed slurry reactor, Ind. Eng. Chem. Res. 46 (2007) 43–51.
[11] J. Colina Marquez, F. Machuca Martinez, G. Li Puma, Radiation absorption and optimization of solar photocatalytic reactors for environmental applications, Environ. Sci. Technol. 44 (2010) 5112–5120.
[12] G. Li Puma, V. Puddu, H.K. Tsang, A. Gora, B. Toepfer, Photocatalytic oxidation of multicomponent mixtures of estrogens estrone (E1), 17-estradiol (E2), 17a-ethynylestradiol (EE2) and estriol (E3) under UVA and UVC radiation: photon absorption, quantum yields and rate constants independent of photon absorption, Appl. Catal. B 99 (2010) 388–397.
[13] M. Motegh, J. Cen, P.W. Appel, J.R. van Ommen, M.T. Kreutzer, Photocatalytic-reactor efficiencies and simplified expressions to assess their relevance in kinetic experiments, Chem. Eng. J. 207–208 (2012) 607–615.
[14] J.E. Cooper, E.L. Kendig, S.M. Belcher, Assessment of bisphenol A released from reusable plastic, aluminium and stainless steel water bottles, Chemosphere 85 (2011) 943–947.
[15] D.P. Mohapatra, S.K. Brar, R.D. Tyagi, R.Y. Surampalli, Physico-chemical pre-treatment and biotransformation of wastewater and wastewater sludge – fate of bisphenol A, Chemosphere 78 (2010) 923–941.
[16] Y.Q. Huang, C.K.C. Wong, J.S. Zheng, H. Bouwman, R. Barra, B. Wahlström, L. Neretin, M.H. Wong, Bisphenol A (BPA) in China: a review of sources,

environmental levels, and potential human health impacts, Environ. Int. 42 (2012) 91–99.
[17] E.J. Rosenfeldt, K.G. Linden, Degradation of endocrine disrupting chemicals bisphenol A, ethinyl estradiol, and estradiol during UV photolysis and advanced oxidation processes, Environ. Sci. Technol. 38 (2004) 5476–5483.
[18] I. Gültekin, N.H. Ince, Synthetic endocrine disruptors in the environment and water remediation by advanced oxidation processes, J. Environ. Manage. 85 (2007) 816–832.
[19] J.C. Sin, S.M. Lam, A.R. Mohamed, K.T. Lee, Degrading endocrine disrupting chemicals from wastewater by TiO_2 photocatalysis: a review, Int. J. Photoenergy (2012) (article ID 185159).
[20] Y. Ohko, I. Ando, C. Niwa, T. Tatsuma, T. Yamamura, T. Nakashima, Y. Kubota, A. Fujishima, Degradation of bisphenol A in water by TiO_2 photocatalyst, Environ. Sci. Technol. 35 (2001) 2365–2368.
[21] T.-W. Kim, M.-J. Lee, W.-G. Shim, J.-W. Lee, T.-Y. Kim, D.-H. Lee, H. Moon, Adsorption and photocatalytic decomposition of organic molecules on carbon-coated TiO_2, J. Mater. Sci. 43 (2008) 6486–6494.
[22] C. Guo, M. Ge, L. Liu, G. Gao, Y. Feng, Y. Wang, Directed synthesis of mesoporous TiO_2 microspheres: catalysts and their photocatalysis for bisphenol A degradation, Environ. Sci. Technol. 44 (2010) 419–425.
[23] N. Venkatachalam, A. Vinu, S. Anandan, B. Arabindoo, V. Murugesan, Visible light active photocatalytic degradation of bisphenol-A using nitrogen doped TiO_2, J. Nanosci. Nanotechnol. 6 (2006) 2499–2507.
[24] X. Wang, T.-T. Lim, Solvothermal synthesis of C–N codoped TiO_2 and photocatalytic evaluation for bisphenol A degradation using a visible light irradiated LED photoreactor, Appl. Catal. B 100 (2010) 355–364.
[25] M.I. Cabrera, O.M. Alfano, A.E. Cassano, Absorption and scattering coefficients of titanium dioxide particulate suspensions in water, J. Phys. Chem. 100 (1996) 20043–20050.
[26] M.L. Satuf, R.J. Brandi, A.E. Cassano, O.M. Alfano, Experimental method to evaluate the optical properties of aqueous titanium dioxide suspensions, Ind. Eng. Chem. Res. 44 (2005) 6643–6649.
[27] W.-T. Tsai, M.-K. Lee, T.-Y. Su, Y.- M. Chang, Photodegradation of bisphenol A in a batch TiO_2 suspension reactor, J. Hazard. Mater. 168 (2009) 269–275.
[28] S.L. Murov, I. Carmichael, G.L. Hug, Handbook of Photochemistry, second ed., Marcel Dekker, New York, 1993.
[29] M.N. Özişik, Radiative Transfer and Interactions with Conduction and Convection, Wiley, New York, 1973.
[30] R. Siegel, J.R. Howell, Thermal Radiation Heat Transfer, fourth ed., Hemisphere Publishing Corp., Bristol, PA, 2002.
[31] M.L. Satuf, M.J. Pierrestegui, L. Rossini, R.J. Brandi, O.M. Alfano, Kinetic modeling of azo dyes photocatalytic degradation in aqueous TiO_2 suspensions. Toxicity and biodegradability evaluation, Catal. Today 161 (2011) 121–126.
[32] R.J. Brandi, O.M. Alfano, A.E. Cassano, Rigorous model and experimental verification of the radiation field in a flat plane solar collector simulator employed for photocatalytic reactions, Chem. Eng. Sci. 54 (1999) 2817–2827.
[33] R.J. Brandi, M.A. Citroni, O.M. Alfano, A.E. Cassano, Absolute quantum yields in photocatalytic slurry reactors, Chem. Eng. Sci. 58 (2003) 979–985.
[34] J. Ryu, W. Choi, Substrate-specific photocatalytic activities of TiO_2 and multiactivity test for water treatment application, Environ. Sci. Technol. 42 (2008) 294–300.